Carrier compensation and scattering mechanisms in Si-doped $InAs_yP_{1-y}$ layers grown on InP substrates using intermediate $InAs_yP_{1-y}$ step-graded buffers

M. K. Hudait,[a] Y. Lin, and P. M. Sinha[b]
Department of Electrical and Computer Engineering, The Ohio State University, Columbus, Ohio 43210

J. R. Lindemuth
Lake Shore Cryotronics, Inc., 575 McCorkle Boulevard, Westerville, Ohio 43082

S. A. Ringel[c]
Department of Electrical and Computer Engineering, The Ohio State University, Columbus, Ohio 43210

(Received 25 January 2006; accepted 8 June 2006; published online 22 September 2006)

Electronic transport properties of strain-relaxed Si-doped $InAs_yP_{1-y}$ layers with arsenic mole fractions between $y=0.05$ and $y=0.50$ were studied. All layers were grown on semi-insulating InP substrates by solid source molecular beam epitaxy using intermediate $InAs_yP_{1-y}$ step-graded buffers to reduce dislocation density. Variable magnetic field (0–8.5 T) Hall effect measurements in conjunction with quantitative mobility spectrum analysis in the temperature range of 25–300 K were used to extract individual carrier mobilities, densities, and donor ionization energy as a function of temperature and alloy composition. The low field mobility is calculated by taking into account various scattering mechanisms, and these results are compared with the experimental results. At a constant electron carrier concentration of $\sim 2\times 10^{16}$ cm^{-3}, the 300 K carrier mobility increases from 2856 to 5507 $cm^2/V\,s$ with increasing arsenic mole fraction from 0.05 to 0.50. The experimental mobilities are in close agreement with the theoretical results using various scattering mechanisms. Both optical polar phonon scattering and ionized impurity scattering are important at 300 K while at 100 K, ionized impurity scattering is the limiting process. Alloy scattering is found to be only of second order importance. The Si donor ionization energy was determined to be $\sim 2-4$ meV for all alloy compositions. © *2006 American Institute of Physics*.
[DOI: 10.1063/1.2349358]

I. INTRODUCTION

InAsP alloys are of growing interest due to their ability to provide a high quality metamorphic buffer system that can enable devices that require "virtual" substrate lattice constants greater than that of InP substrates. Such devices include InGaAs thermophotovoltaic (TPV) cells,[1–6] infrared amplifier and detectors,[7–9] and high-speed InGaAs-based heterojunction bipolar transistors (HBTs).[10] To date, however, there has been relatively little investigation of the electronic transport properties of InAsP and, in particular, with regard to the effects of alloy composition, impurities, and lattice mismatch on carrier mobility. Prior work has focused on single, mismatched InAsP layers grown on InP without benefit of dislocation filtering graded buffers.[11–18] The presence of varying defect density and different degrees of residual strain present in such structures can give rise to ambiguity with regard to interpreting carrier transport in these alloys. Given the rapidly increasing interest in InAsP for device applications that has been enabled by improved capabilities in InAsP graded buffer growth, careful evaluation of carrier transport in high structural quality InAsP alloys is of interest. This paper presents a detailed study of the electron transport properties in Si-doped $InAs_yP_{1-y}$ layers for arsenic mole fractions between $y=0.05$ and $y=0.50$ that are grown by solid source molecular beam epitaxy (MBE) on semi-insulating InP substrates using intermediate unintentionally doped (UID) $InAs_yP_{1-y}$ step-graded buffers. Variable magnetic field Hall effect measurements (0–8.5 T) in conjunction with quantitative mobility spectrum analysis (QMSA®) in the temperature range of 25–300 K were used to extract individual carrier mobilities, carrier concentrations, compensation, and Si ionization activation as a function of alloy compositions in $InAs_yP_{1-y}$ alloys. The theoretical low field electron mobilities are calculated for all compositions by taking into account various scattering mechanisms, and these are compared with the experimental results.

II. METHOD OF ANALYSIS

For epitaxial crystal growers, Hall effect measurements are typically carried out to assess the quality and control of doping in semiconductor layers with the Hall mobility as an important figure of merit. The carrier density, n and mobility μ of a n-type semiconductor are determined from the measured Hall coefficient, $R_H(B)$, and the resistivity, $\rho(B)$, using the relations

[a]Present address: Components Research, Intel Corporation, Hillsboro, OR 97124; electronic mail: mantu.k.hudait@intel.com
[b]Present address: Intel Corporation, Hillsboro, OR 97124.
[c]Author to whom correspondence should be addressed; FAX: (614) 292-9562; electronic mail: ringel.5@osu.edu

$$n = \frac{r_H}{qR_H(B)}, \tag{1}$$

and

$$\mu = \frac{1}{nq\rho(B)}, \tag{2}$$

where q is the electronic charge, B is the magnetic field, and r_H is the Hall factor. If we assume for a nondegenerate n-type semiconductor with a single donor level of concentration N_d, a concentration of compensating acceptors N_a, and full ionization conditions at all temperatures of interest, the concentration n_0 of free electrons in the conduction band at given temperature T is given by the solution of[19]

$$\frac{n_0(n_0+N_a)}{N_d-N_a-n_0} = \frac{N_C}{g}\exp\left(-\frac{E_d}{kT}\right). \tag{3}$$

Here, k is the Boltzmann constant, g is the degeneracy factor [$g=2$ for $InAs_yP_{1-y}$ (Ref. 20)], and E_d is the ionization energy of the donor level. The effective density of states in the conduction band in Eq. (3) can be expressed as

$$N_C = 2\left(\frac{2\pi m^* kT}{h^2}\right)^{3/2} = 4.82\times 10^{15}\left(\frac{m^*}{m_0}\right)^{3/2} T^{3/2}, \tag{4}$$

where h is the Planck constant, m_0 is the free electron mass, and m^* is the density of states electron effective mass, which is derived from $m^*=0.023y+0.079(1-y)$ [for $InAs_yP_{1-y}$ at 300 K (Ref. 21)] as a function of arsenic composition. Solving Eq. (3) for n_0 gives[22,23]

$$n_0(T) = 2(N_d-N_a)\left(1+\frac{gN_a}{N_C}\exp\left(-\frac{E_d}{kT}\right)\right. + \left\{\left[1+\frac{gN_a}{N_C}\exp\left(-\frac{E_d}{kT}\right)\right]^2 + \left.\left[\frac{4g(N_d-N_a)}{N_C}\right]\exp\left(-\frac{E_d}{kT}\right)\right\}^{1/2}\right)^{-1}. \tag{5}$$

By obtaining the value for n_0 from experimental measurements as a function of temperature, the values of N_d and N_a in $InAs_yP_{1-y}$ films for each arsenic composition can be determined by numerically fitting Eq. (5) to $n_0(T)$. A convergent solution for (N_a, N_d, and E_d) is obtained when the error between the theoretically and experimentally measured carrier concentrations is minimized, i.e., when the root mean square (rms) $|\Sigma_j[\ln(n_{0j}/n_j)]^2|^{1/2}$ is a minimum value. In this expression, n_{0j} and n_j are the calculated and experimental free concentrations at the temperature T_j, respectively, and the summations extend over all the experimental points for which the curve fitting is attempted.[19] By knowing the acceptor and donor concentrations from this analysis, the compensation ratio $\theta=N_a/N_d$ for each $InAs_yP_{1-y}$ film was determined. This compensation ratio is an important parameter for assessing crystal quality.

For a sample involving more than one type of carrier or layer grown on graded buffer[24] as in this work, the mobility and carrier density calculated from Eqs. (1) and (2) will be averaged over carriers in all layers. In this case, the longitudinal and transverse conductivity tensor components σ_{xx} and σ_{xy}, respectively, can be expressed as a sum over the m species (conductivities of individual carriers are additive) present within this multicarrier system,[24,25]

$$\sigma_{xx}(B) = \sum_{i=1}^{m}\frac{qn_i\mu_i}{1+(\mu_i B)^2}, \tag{6}$$

and

$$\sigma_{xy}(B) = \sum_{i=1}^{m} S_i\frac{qn_i\mu_i^2 B}{1+(\mu_i B)^2}, \tag{7}$$

where n_i and μ_i are the concentration and mobility of ith carrier species, respectively, and S_i is +1 for holes and −1 for electrons. In this procedure, n_i and μ_i are adjustable parameters, which are varied to give the best fit to the experimental dependencies of σ_{xx} and σ_{xy} on B. Also, the number of groups of carriers must be defined in advance, and the carrier density and mobility for each group of carrier are fitting parameters. Clearly, it is difficult to extract meaningful transport properties of an individual layer with this method. To overcome this limitation, we employ the QMSA® approach,[25–31] where the mobilities of multiple groups of carriers can be separated. In this approach, discrete carriers are generalized by a conductivity density function that spreads over a continuous mobility spectrum. The conductivity tensor defined in Eqs. (6) and (7) can be rewritten as an integral form,[29]

$$\sigma_{xx} = \int_{-\infty}^{\infty}\frac{s^p(\mu)+s^n(\mu)}{1+(\mu B)^2}d\mu, \tag{8}$$

and

$$\sigma_{xy} = \int_{-\infty}^{\infty}\frac{[s^p(\mu)-s^n(\mu)]\mu B}{1+(\mu B)^2}d\mu, \tag{9}$$

where $s^p(\mu)$ and $s^n(\mu)$ are the hole and electron conductivity density functions, respectively. From these expressions, we can extract individual carrier mobility and density for multicarrier systems.

The theoretical electron mobility in $InAs_yP_{1-y}$ is calculated by taking into account the individual scattering momentum relaxation time. The important factors that can affect and limit the theoretical mobility in $InAs_yP_{1-y}$ are alloy scattering, optical polar phonon scattering, optical phonon deformation potential, acoustic phonon deformation potential, piezoelectric scattering, and ionized impurity scattering. We have calculated the electron mobility assuming the validity of Matthiessen's rule and that the total mobility can be obtained in the relaxation time approximation. The individual and total mobilities are given by[18,32]

$$\mu_i = \frac{q\langle\tau_m\rangle^i}{m^*} \text{ and } \mu_{\text{total}}^{-1} = \sum_i \mu_i^{-1}, \tag{10}$$

respectively, where $\langle\tau_m\rangle^i$ is the average momentum relaxation time for the ith scattering process as given by[14]

TABLE I. Material parameters for electron transport in $InAs_yP_{1-y}$.

Parameters	InAs	InP	$InAs_yP_{1-y}$	Reference No.
a (Å)	6.0584	5.8688	Linear interpolation	41 and 42
C_{11} (dyn/cm^2)	8.34×10^{11}	1.01×10^{12}	···	41 and 42
C_{12} (dyn/cm^2)	4.54×10^{11}	5.61×10^{11}	···	41 and 42
C_{44} (dyn/cm^2)	3.95×10^{11}	4.56×10^{11}	···	41 and 42
Piezoelectric constant e_{14} (C/m^2)	-4.5×10^{-2}	-3.5×10^{-2}	···	41 and 42
h_{14} (V/cm)	3.54×10^{6}	3.2×10^{6}	Linear interpolation	41 and 42
C_l (dyn/cm^2)	9.98×10^{11}	1.21×10^{12}	Linear interpolation	41
C_t (dyn/cm^2)	3.13×10^{11}	3.64×10^{11}	Linear interpolation	41
ε_r	14.34	12.38	Linear interpolation	41 and 43
ε_∞	11.74	9.35	Linear interpolation	20
m^* at 300 K	$0.023m_0$	$0.079m_0$	Linear interpolation	43 and 44
Deformation potential E_A (eV)	5.8	6.8	Linear interpolation	43 and 19
Alloy scattering potential ΔE_{alloy} (eV)	···	···	0.581	16, 44, and 45
Optical phonon Debye temperature θ (K)	337	497	Linear interpolation	20
Mass density (g/cm^3)	5.667	4.81	···	41 and 42
Polar phonon energy $\hbar\omega_0$ (eV)	0.029	0.0426	Linear interpolation	41

$$\langle\tau_m\rangle^i = \frac{4}{3\sqrt{\pi}}\int_0^\infty \tau_m^i(z) z^{3/2}\exp(-z)dz, \tag{11}$$

where z is the electron energy in kT. In order to investigate which scattering mechanisms are predominant over the range of $InAs_yP_{1-y}$ alloy compositions and temperature ranges considered here, the material parameters given in Table I along with Eqs. (10) and (11) are used for this calculation. The relaxation time and corresponding mobility for each scattering process are summarized in Table II. The symbols used for the momentum relaxation time and mobility equations are mentioned in Table I.

III. EXPERIMENTAL PROCEDURE

1.5 μm thick Si-doped, n-type $InAs_yP_{1-y}$ layers with $y=0.05-0.50$ were grown by solid source MBE on (100) semi-insulating InP substrates using unintentional $InAs_yP_{1-y}$ step-graded buffers. These films were grown using single-step, two-step, and three-step $InAs_yP_{1-y}$ step-graded buffers to achieve low dislocation density depending on the composition of the final layer to be evaluated. Table III summarizes the details of each test structure that were characterized in this work. The Si cell temperature was kept constant at 1004 °C for the top InAsP test layer for each alloy composition. The actual arsenic compositions for each layer and corresponding amount of strain relaxation were determined using triple-axis x-ray diffraction and this incorporation was included in Table III. Details of growth procedures can be found elsewhere.[1,33]

Quantitative mobility spectrum analysis[25–31] in conjunction with variable field Hall measurements was made for magnetic fields from 100 G to 85 kG (0.01–8.5 T) to obtain individual carrier mobilities and densities as a function of temperature in the range of 20–300 K. A Van der Pauw sample configuration with four contacts was used to conduct the Hall measurements. Gold wires were heat bonded to Au/Ge/Ni contact pads, providing Ohmic contacts over the measurement temperature range. A value for the Hall factor r_H of unity was used for all calculations. The carrier concentrations were also measured using electrochemical capacitance-voltage (ECV) profiling of $InAs_{0.1}P_{0.9}$, $InAs_{0.2}P_{0.8}$, and $InAs_{0.4}P_{0.6}$ layers as well as unintentionally doped $InAs_yP_{1-y}$ step-graded buffers using 0.5M HCl electrolyte. Figure 1 shows ECV carrier concentration profiles of Si-doped n-type $InAs_yP_{1-y}$ with 10%, 20%, and 40% arsenic compositions grown on InP substrates using unintentionally doped $InAs_yP_{1-y}$ step-graded buffers. From this figure, we establish that the electron concentration of each test layer is uniform with $n\sim2\times10^{16}$ cm^{-3} for each composition as desired for the mobility study presented here. One can also see that the interface between the Si-doped $InAs_yP_{1-y}$ layer and undoped $InAs_yP_{1-y}$ buffer layer is clearly indicated.

IV. RESULTS AND DISCUSSION

Temperature dependence variable field Hall measurements and QMSA® spectra

Mobility

To assess the electrical quality of the layer, the carrier concentration and Hall mobilities of the Si-doped $InAs_yP_{1-y}$ ($0<y\leqslant0.50$) layers were measured using variable field Hall measurements by the Van der Pauw method in the measurement temperature range between 25 and 300 K, and the results are analyzed using the QMSA® method. Figures 2(a) and 2(b) show the experimental dependencies of σ_{xx} and σ_{xy} on B at both 300 and 100 K of relaxed InAsP layers with alloy compositions of 10% and 50%. The fitted results from QMSA® of $InAs_yP_{1-y}$ layers with arsenic compositions of 10% and 50% are also included in these figures. The very close fit (solid lines) to the experimental data is a good indication of the quality of the QMSA® method. The qualitative dependencies of σ_{xx} and σ_{xy} on B can be explained in terms of Eqs. (6) and (7). Equation (6) indicates that for a single carrier (i.e., the dominant group of carriers that contribute to the conductivity is from a single layer of the heterostructure)

TABLE II. Momentum relaxation times and corresponding mobility expressions used in calculating the mobility of $InAs_yP_{1-y}$ (Refs. 18, 20, 21, 32, 46, and 47). N_I is total ionized impurity concentration and $\chi(\theta/T)$ is a slow varying function for carriers having *s*-like wave functions appropriate for electrons, and the value of $\chi(\theta/T)$ was selected for a given (θ/T) value from Fig. 4 of Ref. 47 for electrons.

Scattering mechanisms	Momentum relaxation time (τ_m^i)	Mobility (μ_i)
Acoustic phonon deformation potential scattering	$\tau_m^{\mathrm{ADP}} = 2.398\times10^{-20}\left(\frac{C_l}{E_A^2}\right)\left(\frac{m^*}{m_0}\right)^{-3/2}T^{-3/2}z^{-1/2}$	$\mu_{\mathrm{ADP}} = 3.17\times10^{-5}\left(\frac{C_l}{E_A^2}\right)T^{-3/2}\left(\frac{m^*}{m_0}\right)^{-5/2}$
Piezoelectric scattering	$\tau_m^{\mathrm{PE}} = 9.524\times10^{-8}\left[h_{14}^2\left(\frac{4}{C_t}+\frac{3}{C_l}\right)\right]^{-1}T^{-1/2}\left(\frac{m^*}{m_0}\right)^{-1/2}z^{1/2}$	$\mu_{\mathrm{PE}} = 2.522\times10^{8}\left[h_{14}^2\left(\frac{4}{C_t}+\frac{3}{C_l}\right)\right]^{-1}T^{-1/2}\left(\frac{m^*}{m_0}\right)^{-3/2}$
Optical phonon deformation potential scattering	$\tau_m^{\mathrm{ODP}} = 4.83\times10^{-20}\left(\frac{C_l}{E_A^2}\right)\left[\frac{\exp\left(\frac{\theta}{T}\right)-1}{T^{1/2}\theta}\right]\left(\frac{m_0}{m^*}\right)^{3/2}z^{-1/2}$	$\mu_{\mathrm{ODP}} = 6.4\times10^{-5}\left(\frac{C_l}{E_A^2}\right)\left[\frac{\exp\left(\frac{\theta}{T}\right)-1}{T^{1/2}\theta}\right]\left(\frac{m_0}{m^*}\right)^{5/2}$
Optical polar phonon scattering	$\tau_m^{\mathrm{OP}} = \left(\frac{m^*}{2}\right)^{1/2}\frac{\left[\exp\left(\frac{\theta}{T}\right)-1\right]\chi\left(\frac{\theta}{T}\right)}{qE_{\mathrm{OP}}}z^{1/2};$ $E_{\mathrm{OP}} = \frac{m^*q\omega_0\left(\frac{1}{\varepsilon_\infty}-\frac{1}{\varepsilon_0}\right)}{2h}$	$\mu_{\mathrm{OP}} = \frac{8}{3\sqrt{\pi}}\left(\frac{1}{2m^*}\right)^{1/2}\frac{\left[\exp\left(\frac{\theta}{T}\right)-1\right]\chi\left(\frac{\theta}{T}\right)}{E_{\mathrm{OP}}}$
Alloy scattering	$\tau_m^{\mathrm{Alloy}} = \frac{32\sqrt{2}\hbar^4z^{-1/2}}{3\pi(m^*)^{3/2}y(1-y)a^3(\Delta E_{alloy})^2(kT)^{1/2}}$	$\mu_{\mathrm{Alloy}} = \frac{128\sqrt{2}\hbar^4q}{9\pi^{3/2}(m^*)^{5/2}y(1-y)a^3(\Delta E_{\mathrm{alloy}})^2(kT)^{1/2}}$
Ionized impurity scattering	$\tau_m^{\mathrm{ion}} = \frac{16(2m^*)^{1/2}\pi(\varepsilon_0\varepsilon_r)^2(kT)^{3/2}}{N_Iq^4}\left[\ln(1+\gamma^2)-\frac{\gamma^2}{1+\gamma^2}\right]^{-1}z^{3/2};$ $\gamma^2 = 24\frac{m^*(\varepsilon_0\varepsilon_r)(kT)^2}{q^2\hbar^2N_I}$	$\mu_{\mathrm{ion}} = \frac{128(2\pi)^{1/2}\pi(\varepsilon_0\varepsilon_r)^2(kT)^{3/2}}{N_Iq^3(m^*)^{1/2}}\left[\ln(1+\gamma^2)-\frac{\gamma^2}{1+\gamma^2}\right]^{-1}$

to be dominant, σ_{xx} should fall off as B^{-2} in the high magnetic field region, and the divergence of data from this dependence for both experimental and theoretical results indicates the presence of multiple carriers. The corresponding mobility spectrum obtained through the QMSA® procedure is shown in Figs. 3 and 4. Table IV is a summary of the carriers found, along with their mobility, density, and conductivity at each temperature. The mobility is determined by a peak in the conductivity versus mobility spectrum. The total conductivity is the area of the peak, and the carrier density is determined from $\sigma = nq\mu$.[27] From Table IV, we are able to identify those carriers with room temperature carrier density of approximately 2×10^{16} cm^{-3}, which is the carrier density of the Si-doped (top) layer that was independently confirmed by ECV measurements. Hence, for the 10% arsenic composition sample, the dominant carriers that contribute to the carrier density of $\sim2\times10^{16}$ cm^{-3} have an average mobility of $\mu_n \approx 2724$ cm^2/V s at 300 K. For the sample with 50% arsenic composition, the mobility of this dominant group of carriers increases to $\approx$5507 cm^2/V s at 300 K.

TABLE III. $InAs_yP_{1-y}$ (y=0.05–0.50) test structures grown on InP substrates using $InAs_yP_{1-y}$ step-graded buffers.

Sample Number	$InAs_yP_{1-y}$ final layer alloy composition (y)	Lattice mismatch with respect to InP (%)	Number of steps within step-graded buffers	Thickness of each step within step-graded layers (μm)	(%) relaxation of the top $InAs_yP_{1-y}$ layer relative to the substrate from triple axis x-ray diffraction
A	0.05	0.16	1	0.4	~60
B	0.10	0.32	1	0.4	~70
C	0.20	0.65	2	0.4/0.4	~86
D	0.32	1.04	3	0.4/0.4/0.4	~90
E	0.40	1.28	3	0.4/0.4/0.4	~90
F	0.50	1.61	3	0.5/0.5/0.5	~94

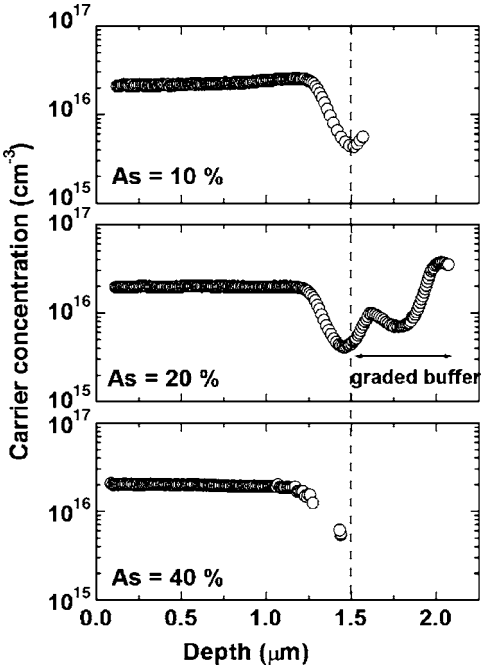

FIG. 1. Electrochemical capacitance-voltage carrier concentration profiles of $InAs_{0.1}P_{0.9}$, $InAs_{0.2}P_{0.8}$, and $InAs_{0.4}P_{0.6}$ layers using 0.5*M* HCl electrolyte.

While the above results show that the mobilities of carriers from solely the top layer can indeed be separated from carriers within the InAsP graded buffer layers using QMSA, the broadness of the 300 K mobility spectra compared to those obtained at lower temperatures, as shown in Figs. 3 and 4, nevertheless reveals the influence of the buried graded buffer layers. Hence, we performed detailed analysis at low temperature measurements to confirm the separation of carrier contributions required to determine mobilities from solely the top layer of these structures. The temperature dependent conductivity versus mobility through QMSA® is included in both Figs. 3 and 4 for the 10% and 50% arsenic composition samples, respectively. Both cases demonstrate the increasing resolution of the peaks with decreasing temperature. This effect is evident for the QMSA® spectrum occurred at 100 and 50 K for the samples with 10% and 50% arsenic compositions, respectively. The majority carrier mobility peak at $\mu_n \approx 2724$ cm^2/V s for the sample with 10% arsenic composition obtained from Fig. 3 measured at 300 K increases to 11 580 cm^2/V s at 100 K. Similarly, the majority carrier mobility peak at $\mu_n \approx 5507$ cm^2/V s for the sample with 50% arsenic composition obtained from Fig. 4 measured at 300 K increases to 12 566 cm^2/V s at 100 K. For all cases, the narrowness of the peak at lower temperatures indicates that the electron mobility must be quite uniform throughout the sample, implying that significant contribution is only from the doped InAsP top layer. Hence, this discussion shows that the mobility of carriers within the buried graded buffer layers does indeed influence the details of the overall mobility spectrum at 300 K and can be completely decoupled at lower measurement temperatures.

In order to further investigate the dependence of the peak electron mobility on both temperature and $InAs_yP_{1-y}$ alloy composition and to provide yet more confidence in our

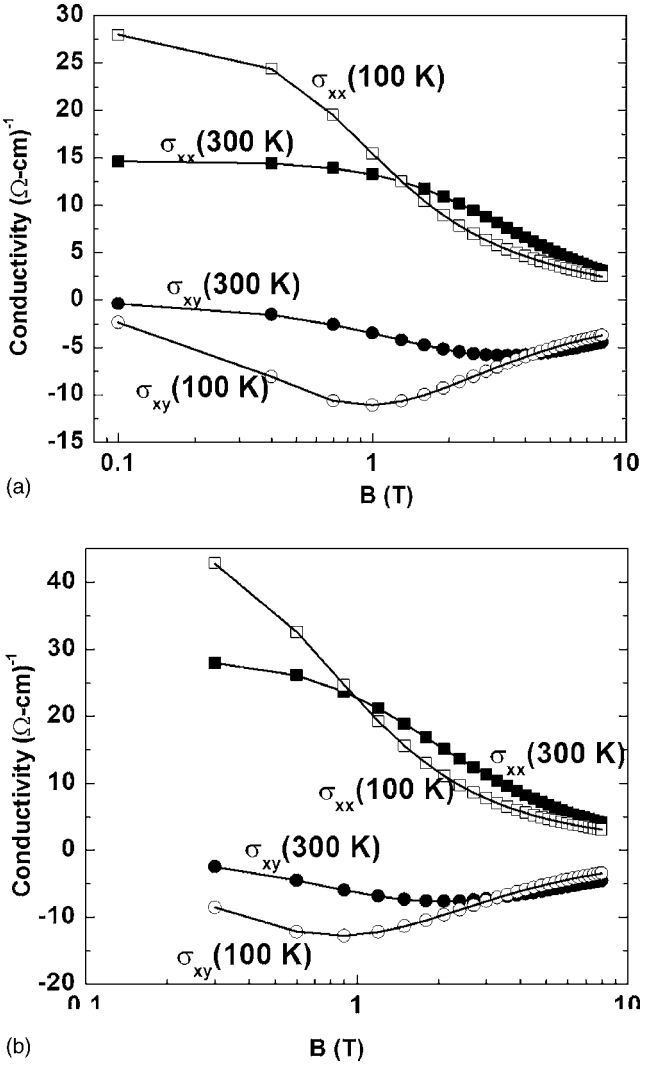

FIG. 2. Experimental values of σ_{xx} (B) and σ_{xy} (B), and corresponding QMSA® fits (solid lines) for both the (a) $InAs_{0.1}P_{0.9}$ and (b) $InAs_{0.5}P_{0.5}$ samples grown on InP using intermediate undoped $InAs_yP_{1-y}$ buffers. Data are shown for each conductivity component at both 300 and 100 K.

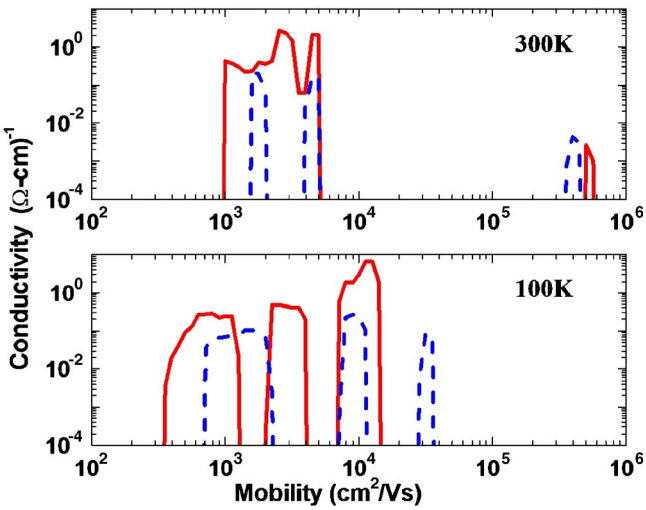

FIG. 3. (Color online) Electron (solid) and hole (dashed) QMSA® spectra of $InAs_{0.1}P_{0.9}$ sample grown on InP using intermediate undoped $InAs_yP_{1-y}$ buffer at 300 and 100 K, respectively.

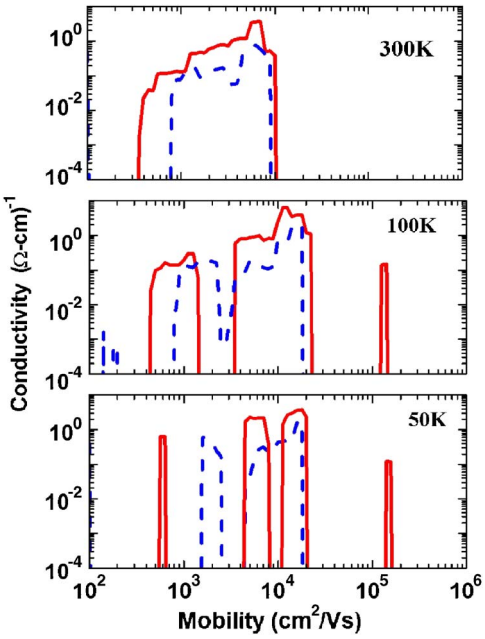

FIG. 4. (Color online) Electron (solid) and hole (dashed) QMSA® spectra of $InAs_{0.5}P_{0.5}$ sample grown on InP using intermediate undoped $InAs_yP_{1-y}$ buffer at 300, 100, and 50 K, respectively.

mobility assignments based on experimentation, a detailed theoretical mobility calculation was performed. The experimental electron mobility of the highest mobility peak determined from QMSA® method for each of the InAsP cap layer compositions and the calculated electron mobility for $InAs_yP_{1-y}$ as a function of arsenic composition are shown in Fig. 5(a) for 300 K. The individual mobility components include (i) alloy scattering (μ_{alloy}), (ii) optical polar phonon scattering (μ_{OP}), (iii) ionized impurity scattering (μ_{ion}), (iv) optical phonon deformation potential (μ_{ODP}), (v) acoustic phonon deformation potential (μ_{ADP}), (vi) piezoelectric scattering (μ_{PE}), and (vii) net mobility (μ_{total}). These component mobilities were calculated using equations from Table II and the material parameters from Table I. There is a good agreement between the experimental and the theoretical results of the total mobility. The electron mobility increases with arsenic composition, as expected, since the electron effective mass decreases systematically from $0.079m_0$ (InP) to $0.023m_0$ (InAs) with increasing arsenic composition. At an electron concentration of $\sim 2\times 10^{16}$ cm^{-3} in the final Si-doped InAsP layer measured by Hall measurement at 300 K, the 300 K carrier mobility increased from 2856 to 5507 cm^2/V s by increasing arsenic sublattice mole fraction y, from 5% to 50%, whereas it increased from 8701 to 12 566 cm^2/V s at 100 K, as shown in Fig. 5(b). One finds from Fig. 5(a) that the polar optical phonon scattering is the primary factor limiting the overall electron mobility. It has been found theoretically that the contribution of ionized impurity scattering to the total mobility is not significant for an ionized impurity concentration of $N_I \leqslant 10^{17}$ cm^{-3}, as can be seen from Table II, in which an impurity concentration of $N_I \cong 10^{17}$ cm^{-3} was used for the calculation. As the temperature decreases, the total electron mobility increases and now the ionized impurity scattering becomes the dominant scattering process. The combined scattering processes due to piezoelectric, acoustic phonon deformation, and optical phonon deformation potentials to the net mobility are less significant at both 300 and 100 K over the entire range of arsenic compositions studied here. From Figs. 5(a) and 5(b), alloy scattering does not appear to be an important factor for carrier mobilities in the $InAs_yP_{1-y}$ having compositions between $y=0.05$ and 0.50. This finding is in apparent contrast with earlier work[15,16] on highly mismatched, single-step InAsP layers grown directly onto InP without benefit of a relaxed, graded buffer layer to yield a high structural quality final layer with a minimum of dislocations.[1,33] Other works in fact, show that direct growth of high mismatched layers can have substantial effects on the mechanism of strain relaxation with respect to issues such as lattice tilt and directionally asymmetric relaxation.[34–36] At

TABLE IV. Summary of electron carriers from QMSA®method.

$InAs_{0.1}P_{0.9}$					
300 K			100 K		
μ (cm^2/V s)	Carrier density (cm^{-3})	σ (Ω cm)$^{-1}$	μ (cm^2/V s)	Carrier density (cm^{-3})	σ (Ω cm)$^{-1}$
1175	6.38×0^{15}	1.2	768	1.49×10^{16}	1.83
2724	1.84×10^{16}	8.0	2 745	5.5×10^{15}	2.42
4717	5.56×10^{15}	4.2	11 580	1.19×10^{16}	22.07

$InAs_{0.5}P_{0.5}$								
300 K			100 K			50 K		
μ (cm^2/V s)	Carrier density (cm^{-3})	σ (Ω cm)$^{-1}$	μ (cm^2/V s)	Carrier density (cm^{-3})	σ (Ω cm)$^{-1}$	μ (cm^2/V s)	Carrier density (cm^{-3})	σ (Ω cm)$^{-1}$
2300	6.14×10^{16}	22.62	1 107	9.4×10^{15}	1.66	597	1.33×10^{16}	1.27
5507	2.00×10^{16}	17.64	5 602	4.05×10^{16}	36.34	5 751	1.15×10^{16}	10.6
			12 566	1.54×10^{16}	31.0	15 923	6.56×10^{15}	16.73
						14 9717	1.02×10^{13}	0.25

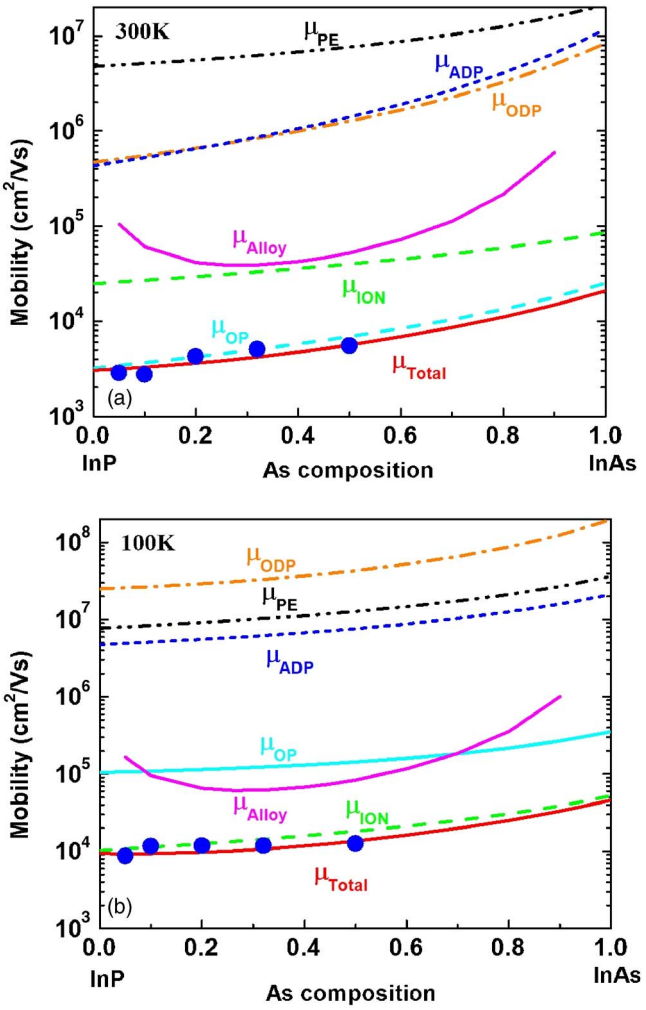

FIG. 5. (Color online) Electron mobility of the individual Si-doped $InAs_yP_{1-y}$ cap layers as a function of arsenic composition obtained through QMSA® analysis at both (a) 300 K and (b) 100 K after elimination of other contributing layers. Also shown are the theoretically calculated individual scattering mobilities; (i) alloy scattering (μ_{alloy}), (ii) optical polar phonon scattering (μ_{OP}), (iii) ionized impurity scattering (μ_{ion}), (iv) optical phonon deformation potential (μ_{ODP}), (v) acoustic phonon deformation potential (μ_{ADP}), (vi) piezoelectric scattering (μ_{PE}), and (vii) the net mobility (μ_{total}). Solid points are experimental data.

present it is not clear what effects these differences may have on the role of alloy scattering. However, the lack of significant alloy scattering may not be surprising since cation-based alloys, such as InGaAs, AlGaAs, or AlGaSb, tend to display much stronger alloy scattering than anion based III-V alloys, and the impact of alloy scattering tends to be diminished for carriers with small effective masses as in the case of InAsP.[37–40] Therefore, polar optical phonon scattering appears to be the primary mobility-limiting factor at 300 K, while at 100 K ionized impurity scattering is an important limiting process, based on the close agreement between experimental analysis and theoretical calculations.

Now that compositional effects have been described, the temperature dependence of the theoretical and experimental electron mobility for a single composition $InAs_{0.5}P_{0.5}$ layers grown using intermediate UID $InAs_yP_{1-y}$ step-graded buffers was considered, and results are shown in Fig. 6. The individual mobilities consist of the same scattering mechanisms

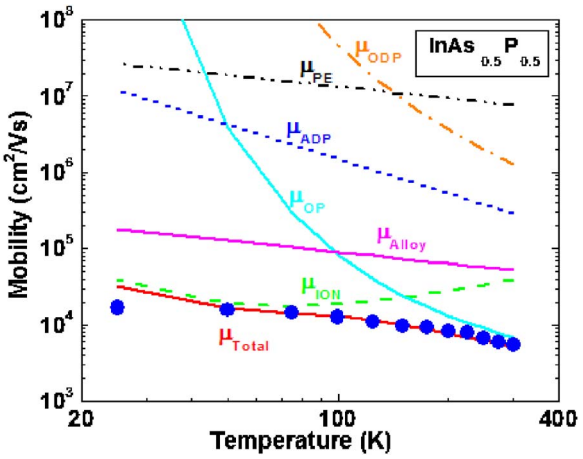

FIG. 6. (Color online) Electron mobility as a function of temperature for an $InAs_{0.5}P_{0.5}$ layer, grown using graded $InAs_yP_{1-y}$/InP substrates, obtained through QMSA® analysis. All calculated scattering mechanisms are plotted along with the experimental results.

shown in Fig. 5, and these are also included in this figure. There is an excellent agreement between the experimental peak electron mobility determined through the QMSA® method as a function of temperature and the theoretical net mobility of this $InAs_{0.5}P_{0.5}$ layer, giving further proof to the validity of QMSA®-based mobility extraction from the top $InAs_{0.5}P_{0.5}$ layer in the presence of the graded buffer discussed earlier. The close agreement between the experimental and theoretical results implies very low carrier compensation and high electronic quality, since the effect of compensation is not considered in the theoretical calculation. At 300 K, the combined effect of both polar optical phonon scattering and ionized impurity scattering dominates the net mobility at this arsenic composition. As the temperature decreases, the total electron mobility increases and the ionized impurity scattering becomes dominant below 100 K as simplistically expected. Contributions from optical, piezoelectric, and acoustic deformation potentials do not appear to be significant at any temperature. The variation of Hall mobility as a function of temperature for each arsenic composition is

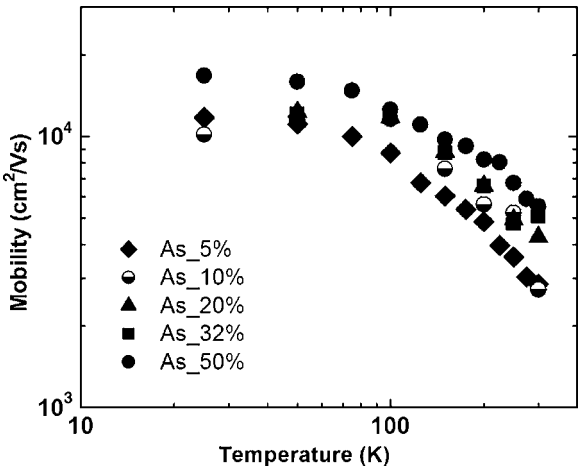

FIG. 7. Electron mobility in Si-doped $InAs_yP_{1-y}$ alloys grown on InP using intermediate undoped $InAs_yP_{1-y}$ buffer as a function of temperature for different alloy compositions.

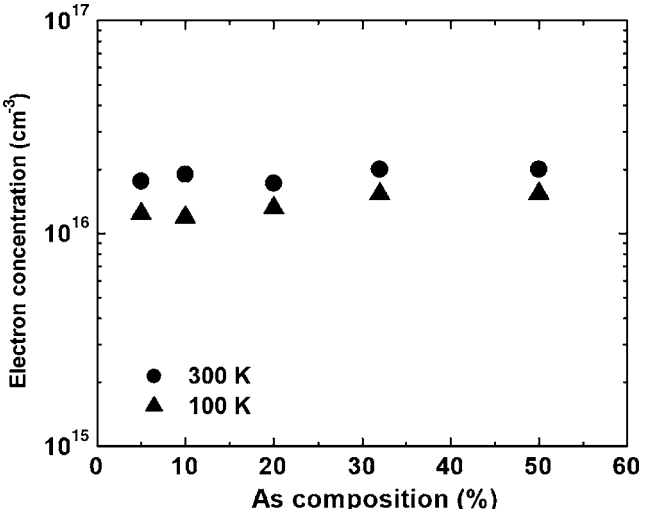

FIG. 8. Measured electron concentration as a function of alloy composition in InAsP at 300 and 100 K.

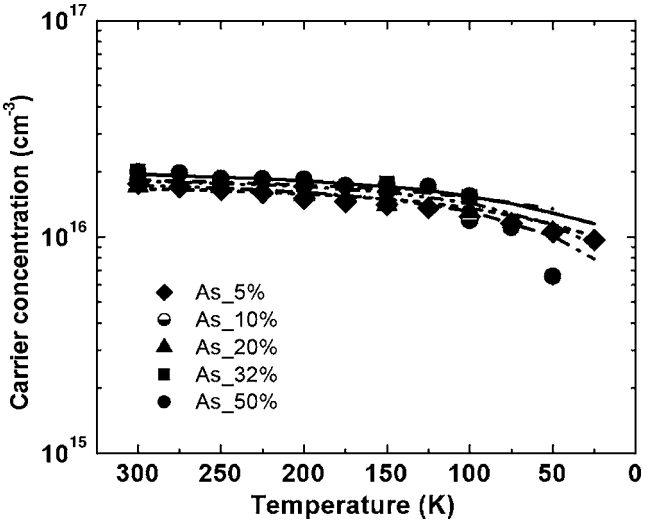

FIG. 9. Experimental and theoretical variations in the electron concentration with temperature for different arsenic compositions in $InAs_yP_{1-y}$ alloys. The line represents the best theoretical fit obtained using Eq. (5) for each arsenic composition in $InAs_yP_{1-y}$ alloys.

shown in Fig. 7, revealing that the mobility increases with increasing arsenic compositions for a fixed temperature, as expected.

Carrier concentration and compensation ratio

The electron concentrations of each of the Si-doped $InAs_yP_{1-y}$ layers as a function of arsenic composition are shown in Fig. 8 at 300 and 100 K. As seen, the Hall-determined electron concentration is $\sim 2\times10^{16}$ cm^{-3} at 300 K and remains nearly constant for all InAsP compositions. The close agreement of the Hall results with the aforementioned ECV results (Fig. 1) also serves to demonstrate the validity of extracting carrier concentrations for doped InAsP layers grown on undoped $InAs_yP_{1-y}$ step-graded buffers on semi-insulating InP substrates. The nearly constant electron concentration values for all alloy compositions (nominally identical Si beam flux during growth of each structure) impy no change in the mechanism and efficiency of Si donor incorporation on the group-III sublattice in $InAs_yP_{1-y}$ alloys for $y=0.05-0.50$.

Figure 9 shows the temperature dependence of carrier concentration as a function of alloy composition from $y=0.05$ to 0.50 in Si-doped $InAs_yP_{1-y}$ layers. Theoretical fitting to the data using Eq. (5) is also plotted in Fig. 9 for all InAsP compositions. The moderately good fit of the theoretical values to the experimental data is evident from a low rms fitting error in the range of 0.03–0.10. The donor ionization energy level that gave the best fit to the experimental data was $E_d=2-4$ meV, which is within the donor ionization energy level range reported for InP ($\sim$6 meV) and InAs ($\sim$1 meV).[41] Table V summarizes the electron concentration, ionization energies, and fitting parameters. The measured carrier concentration n refers to the ionized impurity concentration, and at 300 K it is reasonable to assume that all shallow donors and acceptors are ionized, so that $n=N_d-N_a$. From the fitting process, we can determine N_d and N_a following Eq. (5) from which we can obtain the compensation ratio at each alloy composition. As shown in Table V, the compensation ratios generally decrease from $\sim$0.3–0.35 for more dilute alloys near InP to $\sim$0.02 for $InAs_{0.5}P_{0.5}$ alloy, with all values included in the table. These relatively low compensation ratios imply low concentrations of compensating defects, which are consistent with the high measured mobilities, their match to theoretical calculations, and overall indicate the high electronic quality obtained for relaxed InAsP layers grown using graded InAsP buffers on InP.

V. CONCLUSIONS

Electronic transport properties of MBE-grown, Si-doped $InAs_yP_{1-y}$ layers with $y=0.05-0.50$ on graded $InAs_yP_{1-y}$/InP substrates were studied. Variable magnetic field (0–8.5 T) Hall effect measurements made in conjunc-

TABLE V. Measured electron concentration, mobility, donor ionization energy, and compensation ratio as a function of $InAs_yP_{1-y}$ alloy composition.

$InAs_yP_{1-y}$ alloy composition (y)	n (cm^{-3})		μ (cm^2/V s)		N_d (cm^{-3})	N_a (cm^{-3})	$\theta=N_a/N_d$	E_d (meV)	rms error
	300 K	100 K	300 K	100 K					
5	1.76×10^{16}	1.24×10^{16}	2856	8 701	2.77×10^{16}	9.5×10^{15}	0.34	3.0	0.08
10	1.84×10^{16}	1.19×10^{16}	2724	11 580	2.8×10^{16}	8×10^{15}	0.29	2.0	0.08
20	1.72×10^{16}	1.31×10^{16}	4249	11 789	3.05×10^{16}	1.1×10^{16}	0.36	2.0	0.03
32	2.0×10^{16}	1.53×10^{16}	5062	11 765	2.15×10^{16}	1.5×10^{15}	0.07	4.0	0.05
50	2.0×10^{16}	1.54×10^{16}	5507	12 566	2.24×10^{16}	4×10^{15}	0.02	3.0	0.03

tion with quantitative mobility spectrum analysis (QMSA®) in the temperature range of 25–300 K were used for extraction of individual carrier mobilities and densities. The low field mobility is calculated by taking into account various scattering mechanisms, and these results are compared with the experimental results. At a constant electron carrier concentration of $\sim 2\times 10^{16}$ cm^{-3}, the 300 K carrier mobility increases from 2856 to 5507 cm^2/V s with increasing arsenic mole fraction from 0.05 to 0.50. The experimental mobilities are in close agreement with the theoretical results using various scattering mechanisms. Both optical polar phonon scattering and ionized impurity scattering are important at 300 K while at 100 K, only ionized impurity scattering is the limiting process. Alloy scattering is found to be only secondary in importance. The Si donor ionization energy was determined to be ~2–4 meV for all InAsP alloy compositions studied. Electron mobilities as high as 12 566 cm^2/V s at 100 K for $y=0.50$ with a doping concentration of $\sim 2\times 10^{16}$ cm^{-3} along with a low compensation ratio of 0.02 were observed, indicating that very high electronic quality of relaxed, high arsenic content InAsP layers grown by MBE using step-graded InAsP buffers on InP has been achieved.

ACKNOWLEDGMENT

This work is supported in part by a National Science Foundation Focused Research Group (FRG) Grant No. DMR-0313468.

[1] M. K. Hudait, Y. Lin, M. N. Palmisiano, C. A. Tivarus, J. P. Pelz, and S. A. Ringel, J. Appl. Phys. **95**, 3952 (2004).
[2] M. K. Hudait, Y. Lin, M. N. Palmisiano, and S. A. Ringel, IEEE Electron Device Lett. **EDL-24**, 538 (2003).
[3] M. W. Wanlass *et al.*, AIP Conf. Proc. **460**, 132 (1999).
[4] N. S. Fatemi *et al.*, AIP Conf. Proc. **460**, 121 (1999).
[5] C. S. Murray, F. Newman, S. Murray, J. Hills, D. Aiken, R. Siergiej, B. Wernsman, and D. Taylor, *29th IEEE Photovoltaic Specialists Conference* (IEEE, New York, 2002), p. 888.
[6] R. R. Siergiej *et al.*, AIP Conf. Proc. **653**, 414 (2003).
[7] A. Krier, D. Chubb, S. E. Krier, M. Hopkinson, and G. Hill, IEE Proc.: Optoelectron. **145**, 292 (1998); R. U. Martinelli, T. J. Zamerowski, and P. A. Longeway, Appl. Phys. Lett. **54**, 277 (1989).
[8] M. D'Hondt, I. Moreman, P. Van Daele, and P. Demeester, IEE Proc.: Optoelectron. **144**, 277 (1997).
[9] K. R. Linga, G. H. Olen, V. S. Ban, A. M. Joshi, and W. F. Kosonocky, J. Lightwave Technol. **10**, 1050 (1992).
[10] M. D. Lange, A. Cavus, C. Monier, R. S. Sandhu, T. R. Block, V. F. Gambin, D. J. Sawdai, and A. L. Gutierrez-Aitken, J. Vac. Sci. Technol. B **22**, 1570 (2004).
[11] A. G. Thompson and J. W. Wagner, J. Phys. Chem. Solids **32**, 2613 (1971).
[12] P. J. Wang and B. W. Wessels, Appl. Phys. Lett. **44**, 766 (1984).
[13] K. H. Haung and B. W. Wessels, J. Cryst. Growth **92**, 547 (1988).
[14] H. Ehrenreich, J. Phys. Chem. Solids **12**, 97 (1959).
[15] V. W. L. Chin, J. Phys. Chem. Solids **53**, 897 (1992).
[16] V. W. L. Chin, J. Phys. Chem. Solids **52**, 1193 (1991).
[17] A. El-Sabbathy, A. R. Adams, and M. L. Young, Solid-State Electron. **21**, 83 (1978).
[18] J. W. Harrison and J. R. Hauser, J. Appl. Phys. **47**, 292 (1976).
[19] G. E. Stillman and C. M. Wolfe, Thin Solid Films **31**, 69 (1976).
[20] D. L. Rode, in *Transport Phenomena*, Semiconductors and Semimetals Vol. 10, edited by R. K. Willardson and A. C. Beer (Academic, New York, 1975), p. 1.
[21] S. Adachi, J. Appl. Phys. **53**, 8775 (1982).
[22] D. A. Anderson and N. Apsley, Semicond. Sci. Technol. **1**, 187 (1986).
[23] A. W. R. Leitch, J. Appl. Phys. **65**, 2357 (1989).
[24] R. L. Petritz, Phys. Rev. **110**, 1254 (1958).
[25] J. R. Meyer, C. A. Hoffman, F. J. Bartoli, D. J. Arnold, S. Sivananthan, and J. P. Faurie, Semicond. Sci. Technol. **8**, 805 (1993).
[26] J. Antoszewski, D. J. Seymour, L. Faraone, J. R. Meyer, and C. A. Hooman, J. Electron. Mater. **24**, 1255 (1995).
[27] J. R. Meyer, C. A. Hoffman, J. Antosewski, and L. Faraone, J. Appl. Phys. **81**, 709 (1997).
[28] I. Vurgaftman, J. R. Meyer, C. A. Hoffman, D. Redfern, J. Antoszewski, L. Faraone, and J. R. Lindmuth, J. Appl. Phys. **84**, 4966 (1998).
[29] W. A. Beck and J. R. Anderson, J. Appl. Phys. **62**, 541 (1987).
[30] J. Antoszewski *et al.*, Mater. Sci. Eng., B **44**, 65 (1997).
[31] Z. Dziuba and M. Gorska, J. Phys. III **2**, 99 (1992).
[32] B. R. Nag, *Electron Transport in Compound Semiconductors* (Springer, New York, 1980).
[33] M. K. Hudait, Y. Lin, D. M. Wilt, C. A. Tivarus, E. R. Heller, J. P. Pelz, and S. A. Ringel, Appl. Phys. Lett. **82**, 3212 (2003).
[34] T. Okada, R. V. Kruzelecky, G. C. Weatherly, D. A. Thompson, and B. J. Robinson, Appl. Phys. Lett. **63**, 3194 (1993).
[35] T. Marschner, M. R. Leys, H. Vonk, and J. H. Wolter, Physica E (Amsterdam) **2**, 873 (1998).
[36] S.-W. Ryu, H.-D. Kim, S.-K. Park, W. G. Jeong, and B.-D. Choe, Jpn. J. Appl. Phys., Part 2 **36**, L79 (1997).
[37] D. Chattopadhyay, S. K. Sutradhar, and B. R. Nag, J. Phys. C **14**, 891 (1981).
[38] D. C. Look, D. K. Lorance, J. R. Sizelove, C. E. Stutz, K. R. Evans, and D. W. Whitson, J. Appl. Phys. **71**, 260 (1992).
[39] A. K. Saxena, Phys. Rev. B **24**, 3295 (1981); J. Appl. Phys. **58**, 2640 (1985).
[40] A. H. Ramelan and E. M. Goldys, J. Appl. Phys. **92**, 6051 (2002).
[41] M. P. Mikhailova and N. M. Shmidt, in *Handbook Series on Semiconductor Parameters*, edited by M. Levinshtein, S. Rumyantsev, and M. Shur (World Scientific, River Edge, NJ, 1996), Vol. 1, Chaps. 7 and 8.
[42] O. Madelung, *Semiconductors. Basic Data* (Springer-Verlag, Berlin, 1996).
[43] W. Walukiewicz, J. Lagowski, L. Jastrzebski, P. Rava, M. Lichtensteiger, C. H. Gatos, and H. C. Gatos, J. Appl. Phys. **51**, 2659 (1980).
[44] J. R. Hauser, M. A. Littlejohn, and T. H. Glisson, Appl. Phys. Lett. **28**, 458 (1976).
[45] M. A. Littlejohn, J. R. Hauser, T. H. Glisson, D. K. Ferry, and J. W. Harrison, Solid-State Electron. **21**, 107 (1978).
[46] C. M. Wolfe, G. E. Stillman, and W. T. Lindley, J. Appl. Phys. **41**, 3088 (1970).
[47] D. Kranzer, Phys. Status Solidi A **26**, 11 (1974).